Fully kinetic simulation study of ion-acoustic solitons in the presence of trapped electrons

S. M. Hosseini Jenab* and F. Spanier†

Centre for Space Research, North-West University, Potchefstroom Campus, Private Bag X6001, Potchefstroom 2520, South Africa

(Received 24 August 2016; revised manuscript received 15 February 2017; published 2 May 2017)

The nonlinear fluid theory developed by Schamel suggests a modified KdV equation to describe the temporal evolution of ion acoustic (IA) solitons in the presence of trapped electrons. The validity of this theory is studied here by verifying solitons' main characteristic, i.e., stability against successive mutual collisions. We have employed a kinetic model as a more comprehensive theory than the fluid one, and utilized a fully kinetic simulation approach (both ions and electrons are treated based on the Vlasov equation). In the simulation approach, these solitons are excited self-consistently by employing the nonlinear process of IA solitons formation from an initial density perturbation (IDP). The effect of the size of IDPs on the chain formation is proved by the simulation code as a benchmark test. It is shown that the IA solitons, in the presence of trapped electrons, can retain their features (both in spatial and velocity direction) after successive mutual collisions. The collisions here include encounters of IA solitons with the same trapping parameter, while differing in size. Kinetic simulation results reveal a complicated behavior during a collision between IA solitons in contrast to the fluid theory predictions and simulations. In the range of parameters considered here, two oppositely propagating solitons rotate around their collective center in the phase space during a collision, independent of their trapping parameters. Furthermore, they exchange some portions of their trapped populations.

DOI: 10.1103/PhysRevE.95.053201

I. INTRODUCTION

The ion-acoustic (IA) solitons were first discovered in the context of nonlinear fluid theory by Washimi and Taniuti [1]. These nonlinear modes, localized structures, possess two characteristics:

(1) propagation without change in their features, such as velocity, shape, and size (e.g., width and height).

(2) stability against (theoretically infinite number of) mutual collisions.

The IA solitons have been observed both in laboratory experiments [2] and in a wide range of space plasma observations [3–5]. Fluid theory predicts the existence condition for solitons called nonlinear dispersion relation (NDR), which is, in fact, a sensitive relationship among different features of solitons, e.g., velocity and size. Any localized structure with values other than what is dictated by NDR is expected to break into N-solitons in a long-term evolution. The existence of N-soliton solution for the KdV equation has been proven with different mathematical approaches starting by the seminal work of Hirota [6,7]. In this paper, by harnessing this phenomenon, i.e., chain formation, self-consistent IA solitons are produced from an initial density perturbation (IDP).

Schamel [8–10] has developed a modified KdV (mKdV) equation, by extending the work of Washimi and Taniuti [1] to include the trapping effect of electrons. Based on β (*trapping parameter*), the distribution function of trapped electrons can take three different types of shapes, namely *hollow* ($\beta < 0$), *plateau* ($\beta = 0$), and *hump* ($\beta > 0$). Schamel has identified three regimes considering the trapping effect [8]. For $\beta = 1$, the KdV regime recovers from mKdV solutions. For $\beta_c < \beta < 1$ and $\beta < \beta_c$, two modified KdV regimes are proposed with their own distinctive IA solitons, namely Schamel-KdV and Schamel, respectively. β_c depends on the amplitude of the IA soliton and stays below $\beta_c < 1.0$.

This study is an attempt to verify Schamel's theory and its prediction about IA solitons in the presence of trapped electrons, based on a fully kinetic simulation approach for the first time (both electrons and ions dynamics are treated by the Vlasov equation). The second characteristic of (self-consistently excited) IA solitons is addressed for different values of β. The trapping parameter (β) ranges from negative to positive values, covering all three possible shapes of the distribution function of trapped electrons. All three regimes suggested by Schamel are also examined in the chosen range of the trapping parameter. Collisions of the IA solitons are analyzed in both spatial and velocity directions focusing on number density profiles and distribution functions, respectively. However, the study is limited to collisions of IA solitons with the same trapping parameter.

There have been a few simulation studies considering IA solitons. Most of these simulations have utilized fluid-based simulations (either KdV or fully fluid) [11,12], which can't include the trapping effect accurately. In the case of hybrid-PIC simulations, the trapping effect of electrons are mostly ignored by assuming electrons as a Boltzmann's fluid [13]. Kakad *et al.* [14] have considered the trapping effect in their PIC simulations. However, they have not studied the trapping effect systematically in the range as wide as the one reported here. Furthermore, the inherit noise in PIC smooths out the details of the distribution function of trapped electrons, destroying trapping effect.

The self-consistent approach to create IA solitons, i.e., chain formation, is tested for small and large amplitude IDPs in Sec. III A. Predictions and simulation results reported by fluid or PIC method are verified [11–14] as a benchmark test. Stability of the IA solitons in the presence of trapped electrons against collisions is addressed in Sec. III B. The kinetic details of the collisions for three different shapes of

*mehdi.jenab@nwu.ac.za
†felix@fspanier.de

the trapped electrons distribution functions are presented in Sec. III C.

II. BASIC EQUATIONS AND NUMERICAL SCHEME

All variables and quantities used in the rest of the text are normalized to dimensionless forms to simplify the equations. Space and time are normalized by λ_{Di} and ω_{pi}^{-1}, respectively, where $\omega_{pi} = \sqrt{n_{i0}e^2/(m_i\epsilon_0)}$ denotes the ion plasma frequency and $\lambda_{Di} = \sqrt{\epsilon_0 K_B T_i/(n_{i0}e^2)}$ is the characteristic ion Debye length. The velocity variable v has been scaled by the ion thermal speed $v_{th_i} = \sqrt{K_B T_i/m_i}$, while the electric field and the electric potential have been reduced by $K_B T_i/(e\lambda_{Di})$ and $K_B T_i/e$, respectively (here, K_B is Boltzmann's constant). The densities of the two species are normalized by n_{i0}, while energy is scaled by $K_B T_i$. In order to introduce an IDP into the simulation domain, the so-called Schamel distribution function [15,16] is used as follows:

$$f_s(v) = \begin{cases} A\exp\left[-\left(\sqrt{\frac{\xi_s}{2}}v_0 + \sqrt{E(v)}\right)^2\right] & \text{if} \begin{cases} v < v_0 - \sqrt{\frac{2E_\phi}{m_s}} \\ v > v_0 + \sqrt{\frac{2E_\phi}{m_s}} \end{cases} \\ A\exp\left[-\left(\frac{\xi_s}{2}v_0^2 + \beta_s E(v)\right)\right] & \text{if} \begin{cases} v > v_0 - \sqrt{\frac{2E_\phi}{m_s}} \\ v < v_0 + \sqrt{\frac{2E_\phi}{m_s}} \end{cases} \end{cases},$$

in which $A = \sqrt{\frac{\xi_s}{2\pi}}n_{0s}$ and $\xi_s = \frac{m_s}{T_s}$ are amplitude and the normalization factor, respectively. $E(v) = \frac{\xi_s}{2}(v - v_0)^2 + \phi\frac{1}{T_s q_s}$ represents the (normalized) energy of particles. v_0 stands for the velocity of the IA soliton. In the set of the simulations presented here, this distribution function has been used to introduce a stationary IDP ($v_0 = 0$) at x_0:

$$\phi = \psi\ \exp\left(\frac{x - x_0}{\Delta}\right)^2, \tag{1}$$

where ψ and Δ are the amplitude and width of the stationary IDP, respectively. It is proven that this distribution function satisfies the continuity and positiveness conditions while producing a trapped population in its phase space [15,16].

The simulation method, employed here, has been developed by the authors based on the method called *Vlasov-hybrid simulation*(VHS), which was initially proposed by Nunn [17] (for details see Refs. [18–20]). It follows the trajectories of the so called *phase points* [21] in the phase space, depending on Liouville's theorem as the theoretical framework. It meets the condition of positiveness of the distribution function during temporal evolution perfectly. Preserving entropy ($\int f \ln f dv dx$) and energy stands as one of the major advantages of the method. In simulations presented in this paper, each plasma species (i.e., electrons and ions) is described by the (scaled) Vlasov equation:

$$\frac{\partial f_s(x,v,t)}{\partial t} + v\frac{\partial f_s(x,v,t)}{\partial x} + \frac{q_s}{m_s}E(x,t)\frac{\partial f_s(x,v,t)}{\partial v} = 0, \quad s = i,e, \tag{2}$$

where $s = i,e$ represents the corresponding species. The variable v denotes velocity in phase space. q_s and m_s are normalized by e and m_i, respectively. Densities of the plasma components are calculated through integration as

$$n_s(x,t) = n_{0s}\int f_s(x,v,t)dv, \tag{3}$$

which are coupled with Poisson's equation:

$$\frac{\partial^2\phi(x,t)}{\partial x^2} = n_e(x,t) - n_i(x,t). \tag{4}$$

The equilibrium values n_{s0} are assumed to satisfy the quasineutrality condition ($n_{e0} = n_{i0}$) at the initial step.

The constant parameters that remain fixed through all of our simulations are $\frac{m_i}{m_e} = 100$, time step $d\tau = 0.01$, $\theta = \frac{T_e}{T_i} = 64$, and $L = 4096$, where L is the length of the simulation box. Perturbation features are either $\psi = 0.05$ and $\Delta = 10$ (small IDP) or $\psi = 0.2$ and $\Delta = 500$ (large IDP). The values of β were modified between successive simulations in range of $-1.0 \leqslant \beta \leqslant 1.0$. We have considered a two-dimensional phase space with one spatial and one velocity axis. The phase space grid (N_x, N_v) size is (4096,4000). The periodic boundary condition is employed on x direction in order to create successive collisions between IA solitons.

III. RESULTS AND DISCUSSION

Before presenting the simulation results, a general overview of their temporal evolution is reported. An initial density perturbation (IDP), which is selected to be around $x/\lambda_{Di} = 512$, is produced in the simulation domain using the Schamel distribution function. First, this IDP breaks into two oppositely drifting density perturbations (DDPs) due to the symmetry in the velocity direction. As the temporal progression continues, each of the DDPs emit their own Langmuir wave packets ahead of itself. These wave packets are much faster than the ionic structures such as DDPs. Therefore, they quickly get separated from the IDPs. Furthermore, the DDPs forms one or more IA solitons with different velocities and sizes, but with the same β as the stationary IDP [22]. The number of IA solitons depends on the value of the trapping parameter as well as the amplitude of IDPs. IA solitons with higher amplitude possess higher velocities, hence the IA solitons are aligned in spatial direction based on their height. Behind the DDPs, ion-acoustic wave packets are created that are slightly slower than the DDPs. The IA wave packets are produced independent from the DDPs.

The solitons and DDPs created from the chain formation are not stationary BGK states. However, they are produced self-consistently, which makes them free from any approximation used in the Schamel's theory derivation of mKDV equations, such as small amplitude. Furthermore, this process resembles the experimental approach used in a double plasma (DP) device to excite solitons [2].

Since the periodic boundary condition is employed on the spatial direction, the wave packets never leave the simulation domain. In long-term simulations, they resonate with each other and cause numerical instabilities so that particles are pushed out of the simulation domain. Hence, the conservation laws are violated. Simulation results presented here are long before the time of the resonance and the conservation laws are checked for deviations to stay below 1% constantly. This

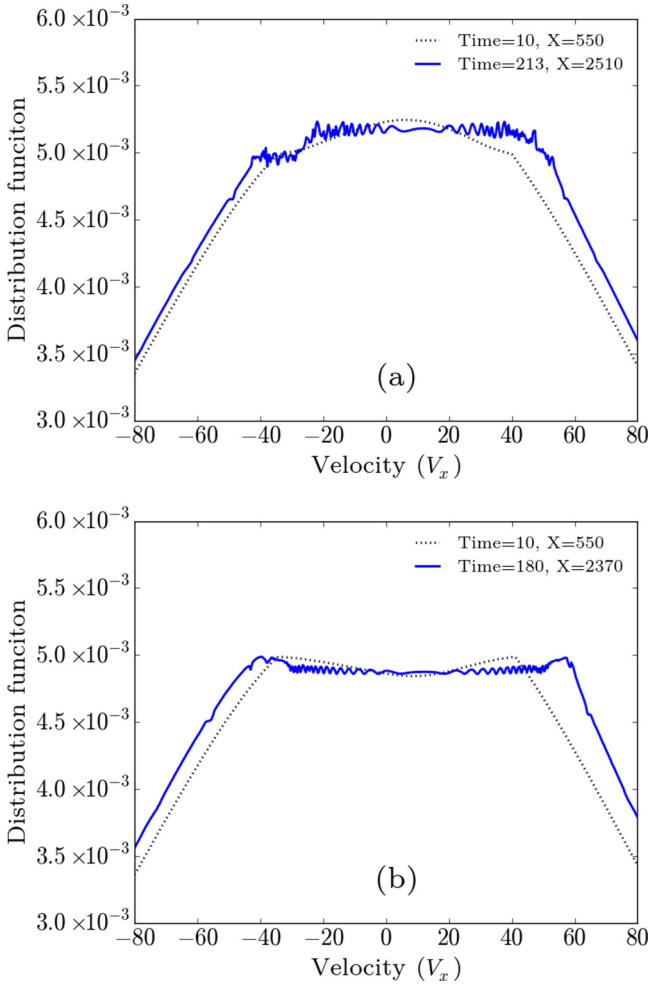

FIG. 1. The evolution of the distribution function versus velocity is shown for $\beta = 0.2$ (a) and $\beta = -0.1$ (b). At $\tau = 10$ the distribution function (black dotted line) is presented at $x = 550$, middle of the DDP, which shows hump (hollow) for $\beta = 0.2$ ($\beta = -0.1$). Blue solid line presents the distribution function at the middle of the first soliton just before its first collision. Filamented structures can be witness to grow inside the distribution function of trapped population.

effect restricts the trapping parameter (β) range, reported in this study. The further the trapping parameter deviates from zero, the stronger wave packets would appear. On the other hand, since the focus is on the collision of the IA solitons, the periodic boundary condition can't be removed. Therefore, here the study is limited to $-1.0 < \beta < 1.0$.

In the early stage of the evolution, before any collisions, the internal structure of solitons in the phase space shows filamentation structures which become finer during temporal progression (Fig. 1).

A. The effect of IDP size

When the amplitude of the DDPs are small enough, they don't disintegrate into a number of IA solitons. Each of the DDPs forms just one IA soliton. Figure 2 shows the simulation results for the case of small IDP ($\psi = 0.05$ and $\Delta = 10$) with $\beta = 0$. The existence of two wave packets, namely, Langmuir and ion-acoustic, can be observed. The Langmuir wave packet

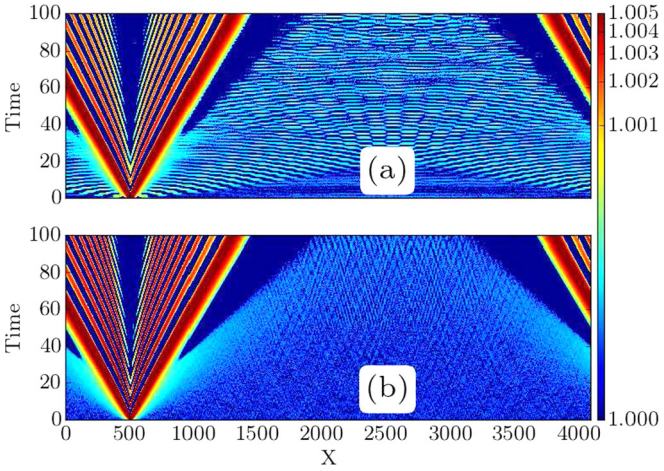

FIG. 2. The temporal evolution of electrons (a) and ions (b) number density, for the case of a small IDP ($\psi = 0.05$, $\Delta = 10$) with $\beta = 0$, is shown. The propagation of both Langmuir and IA wave packets can be witnessed. The number density are shown with color covering values from 1.0 to 1.005. Note that the colors are arranged based on a power-law distribution so the small amplitude Langmuir wave packet in the electron number density can be recognizable.

is recognizable in the electron number density, as waves propagating faster than the DDPs. For the ion number density in the same area, a small-amplitude noise can be recognized. The noise is coming from the effect of Langmuir waves on ions. Since ions don't resonate or participate in propagation of Langmuir waves, there is no wave pattern in the noise. On the other hand, the IA wave packet appears behind the DDPs which is also independent from them. The IA wave packet

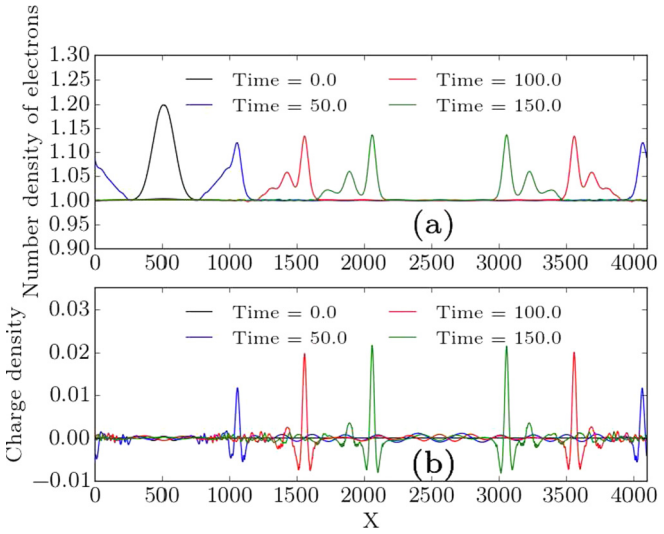

FIG. 3. Profiles of electrons number density (a) and charge density (a) are shown for a large IDP ($\psi = 0.2$, $\Delta = 500$) with $\beta = -0.1$. Four different times during disintegration process, namely, $\tau = 0, 50, 100, 150$, are presented with black (around $x = 500$), blue (around $x = 1000$), red (around $x = 1500$), and green (around $x = 2000$), respectively. The disintegration process of each of DDPs into three IA solitons can be seen in details.

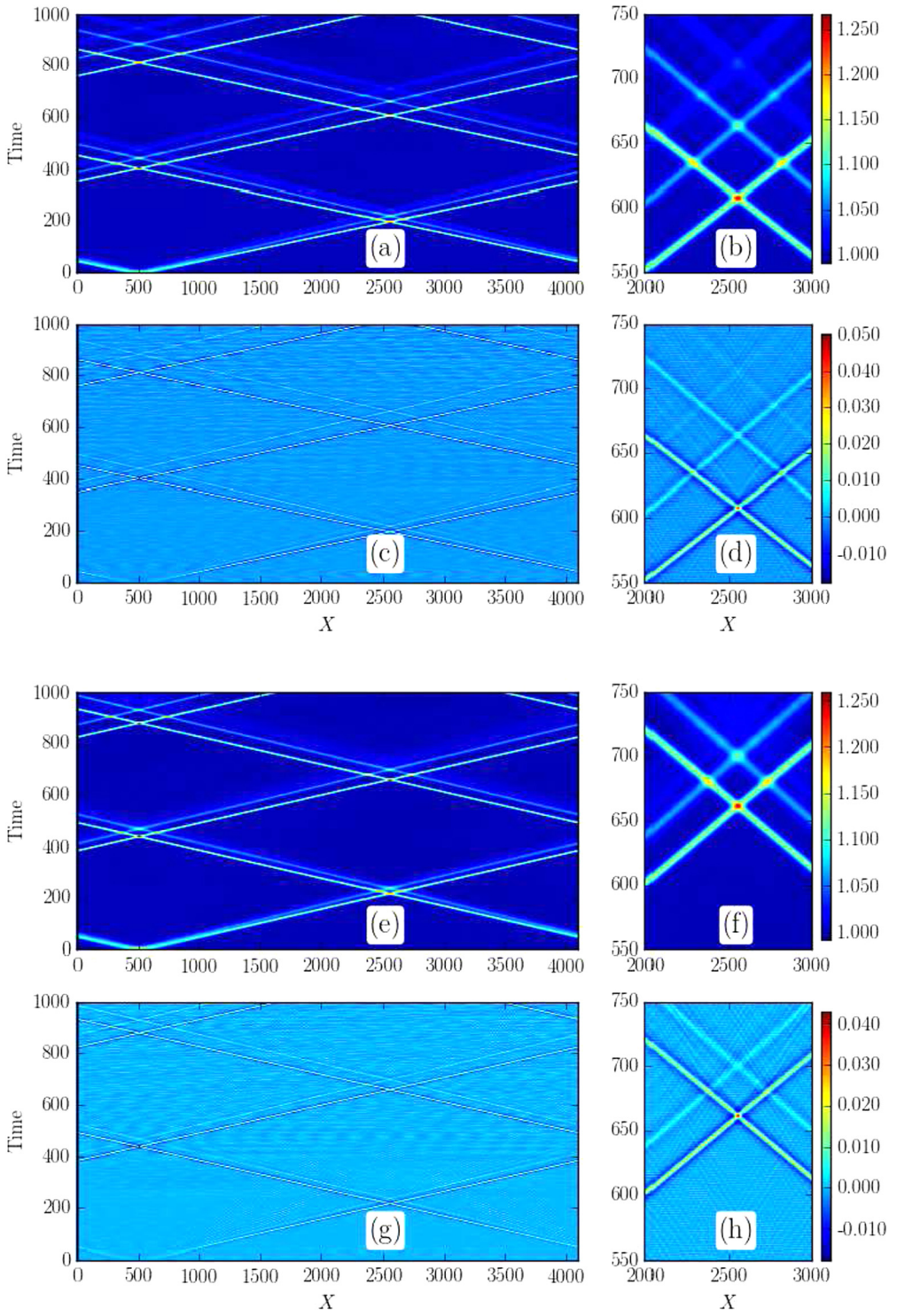

FIG. 4. The temporal evolution of electrons number density and charge density are shown for a large IDP ($\psi = 0.2$, $\Delta = 500$) and two values of β. Panels (a) and (b) represent the electrons number density for $\beta = -0.1$, while (c) and (d) display the charge density for the same value of β. The electrons number density for $\beta = 0.2$ is shown in (e) and (f), while (g) and (h) display the charge density. Twelve (eight) collisions are observed for each of six (four) IA solitons in case of $\beta = -0.1$ ($\beta = 0.2$). Zoomed-in panels (b), (d), (f), and (h) on the right side of each figures display the details of three successive collisions around the time $550 < \tau < 750$. Since the trajectories of solitons don't change by this collisions, hence their velocities are conserved.

starts from the remanence of the initial perturbation when the DDPs have already left it.

Figure 3 presents the results for a large IDP ($\psi = 0.2$ and $\Delta = 500$) with $\beta = -0.1$. The DDPs disintegrate into three solitons. First, the initial stationary IDP breaks into two opposite DDPs. Then, each of the DDPs steepens on their propagation side due to nonlinearity. Furthermore, three IA solitons start surfacing. The earlier they appear (since they

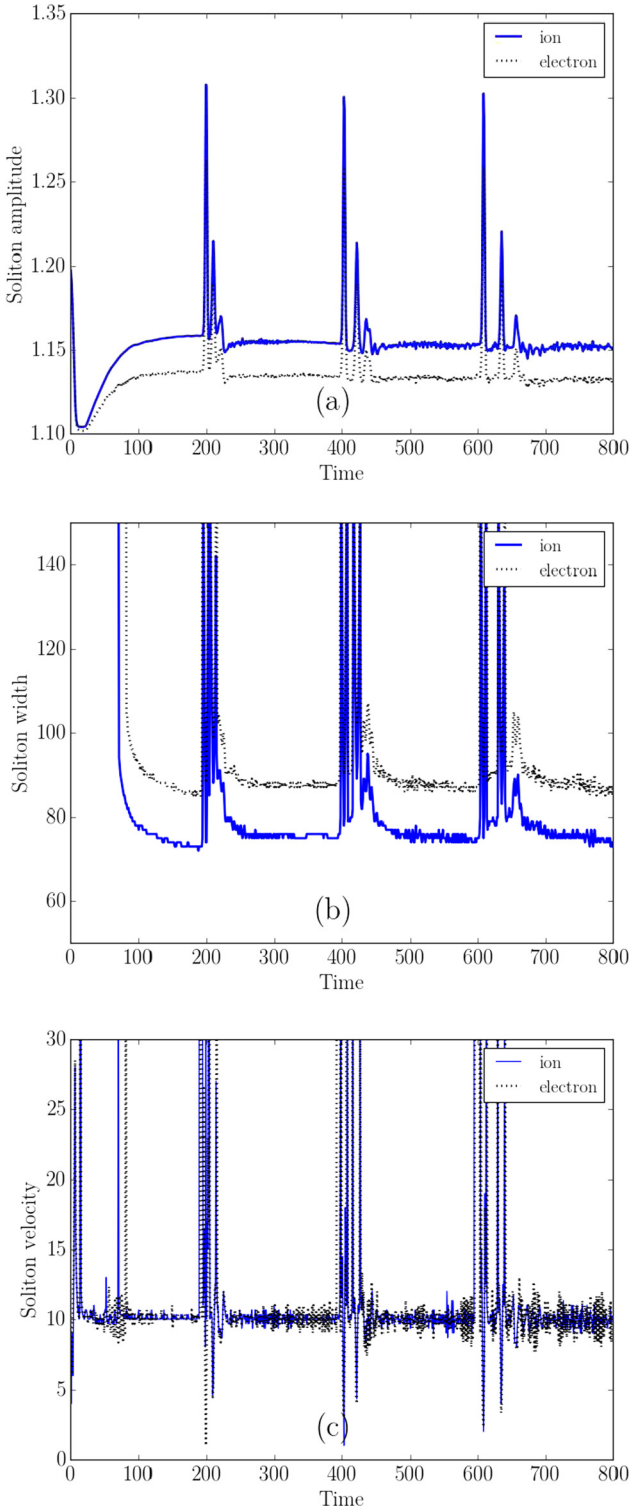

FIG. 5. The temporal evolution of features such as amplitude (a), width (b), and velocity (c) of ions (blue solid line) and electrons (black dotted line) number densities are shown for the right-propagating first and dominant soliton in case of $\beta = -0.1$, $\psi = 0.2$, and $\Delta = 500$. Anomalies take place in the measurement during collision times, i.e., $180 < \tau < 250$, $380 < \tau < 450$, $580 < \tau < 650$. The fluctuation of the values around the average for propagation times (excluding the collision intervals) are less than 1%, 5%, and 8% for amplitude ($1.12 < a_e < 1.14, 1.14 < a_i < 1.16$), width ($85 < w_e < 95$, $70 < w_i < 80$), and velocity ($11.0 < v_i = v_e < 9.0$), respectively.

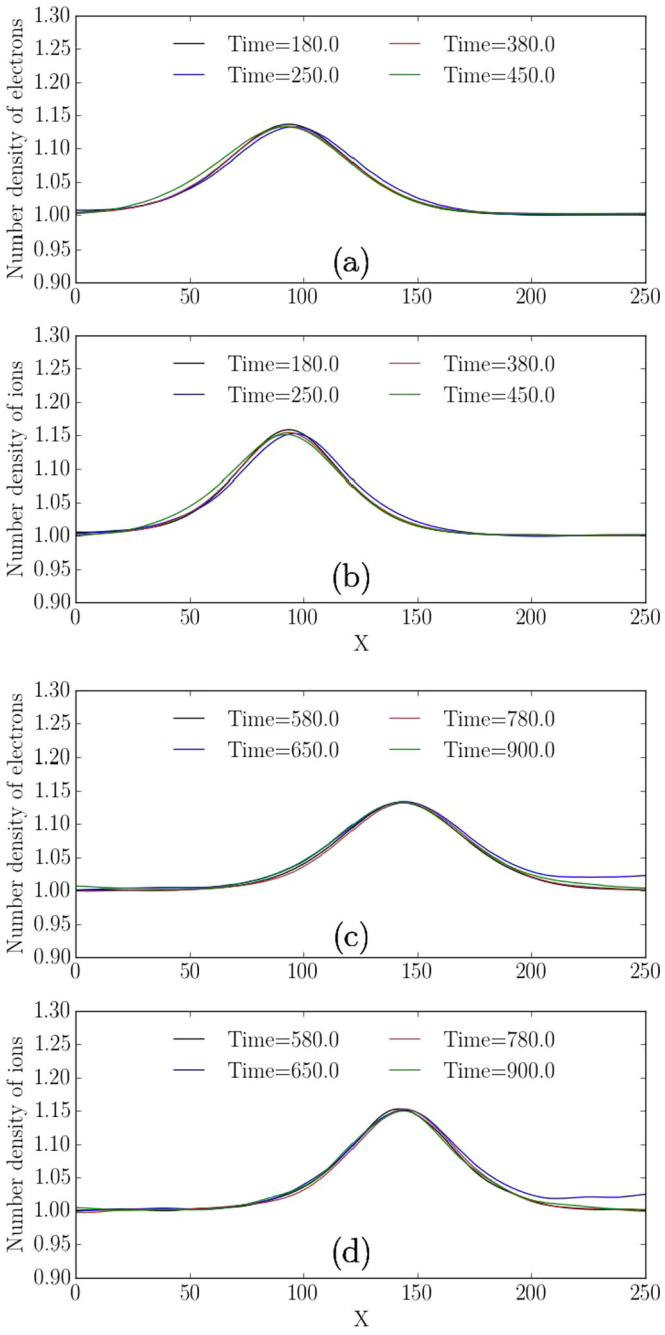

FIG. 6. For a large IDP ($\psi = 0.2$, $\Delta = 500$) with $\beta = -0.1$, the number density profiles of the first and dominant IA soliton are presented for different times. The number density profiles of electrons (a) and ions (b) before and after the first ($\tau = 180$, $\tau = 250$) and the second ($\tau = 380$, $\tau = 450$) triple collision are shown. The same is presented for electrons (c) and ions (d) for the third ($\tau = 580$, $\tau = 650$) and the fourth ($\tau = 780$, $\tau = 900$) triple collisions.

are faster), the more dominant and taller they are. As Fig. 3 shows, the breaking between the first and the associated DDP happens around $\tau = 100$, and the breaking between the second and the third IA solitons takes place later around $\tau = 150$. Note the difference between Figs. 2 and 3, in which the ion-acoustic wave packets are created independent from the DDPs, but the IA solitons are created from the bulk of the DDPs. These results, i.e., (a) the existence of wave packets,

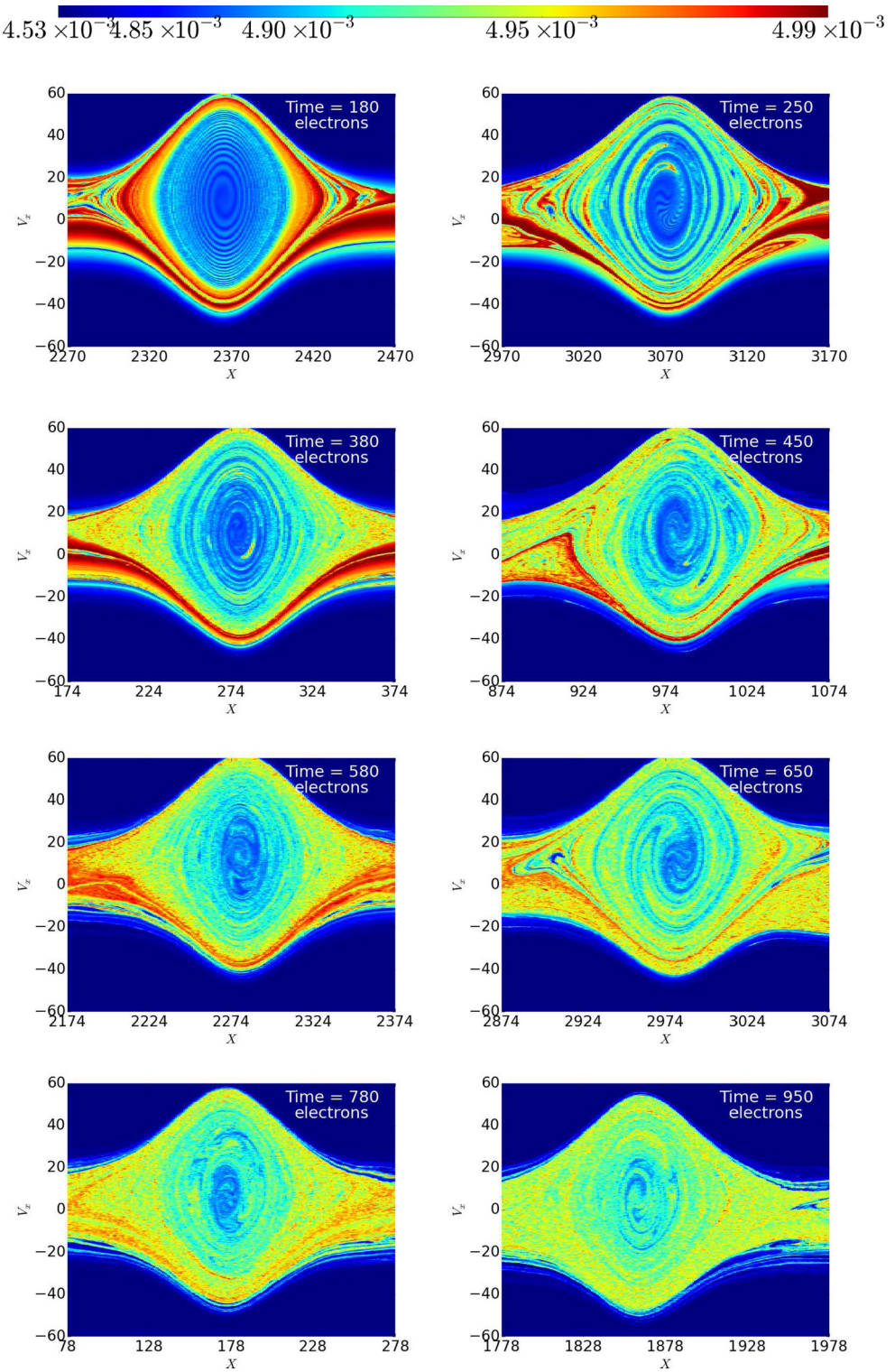

FIG. 7. For the case of large IDP ($\psi = 0.2$ and $\Delta = 500$) and $\beta = -0.1$, the hollow in the electrons' distribution function accompanying the right-propagating first and dominant IA soliton are shown in the phase space. The phase space structure of the trapped population is presented before and after first ($\tau = 180, 250$), second ($\tau = 380, 450$), third ($\tau = 580, 650$), and fourth ($\tau = 780, 900$) triple collisions, respectively, starting from the top left corner. The size and shape of hollows stay the same for all the figures, confirming the stability. However, the symmetry of the hollow (in the phase space) are distorted increasingly as the number of collisions increases. See Supplemental Material [24] for the early stage development of the hollow, i.e., $\tau < 180$.

(b) the breaking of an stationary IDP into two oppositely DDPs, (c) disintegration of a DDP into one or more IA solitons, have been reported in both fluid and PIC simulations as well [11–14].

B. Stability against mutual collisions

Figure 4 demonstrates successive mutual collisions between IA solitons for two cases $\beta = -0.1$ and $\beta = 0.0$ for large IDPs ($\psi = 0.2, \Delta = 500$). In the case of $\beta = -0.1$, each of the DDPs break down into three IA solitons. Each of the these IA solitons has gone through 12 collisions up to $\tau = 1000$. These collisions take place between IA solitons of different sizes with same trapping parameter β. The 12 collisions happen in 4 sets of triple collisions during $180 < \tau < 250$, $380 < \tau < 450$, $580 < \tau < 650$, and $780 < \tau < 900$. In the case of $\beta = 0.2$, two IA solitons emerge from each of the DDPs, and there are 8 collisions.

In order to study the stability of these IA solitons during mutual collisions, different features of them have been considered. Two categories of features have been studied here, i.e., (a) spatial features such as amplitude, width, and shape in the number density profiles and the velocity of propagation, and (b) velocity-direction features like width and shape in phase space.

Figure 5 focuses on three of these spatial features, i.e., amplitude, width, and velocity for the case of trapping parameters with negative values. It shows that they stay the same after the mutual collisions within acceptable margin of error. The collision intervals can be easily recognized within all three figures. What's more, one can observe the initial break-up of IDP ($\tau < 25$) and then steeping of the DDPs before breaking into number of solitons ($25 < \tau < 70$) in the figure reporting temporal evolution of amplitude. Figure 6 presents the number density profiles of the first IA soliton for the case $\beta = -0.1$, hence focusing on shape of solitons and its stability. The electron and ion number density profile of the first right-propagating IA soliton is shown for eight different times before and after each of the triple collisions. The stability of the IA soliton can be observed clearly as its size (including height and width) and shape in the spatial direction don't change. These two figures confirm the stability of spatial features against mutual collisions.

The number densities of plasmas species, as fluid approximation of their distribution functions $N = \int f dv$, serve as a starting point for the fluid theory. Therefore, the stability of their features against mutual collisions prove their fluid-level stability. In other words, kinetic effects such as electron trapping do not alter the stability and the propagation features of IA solitons.

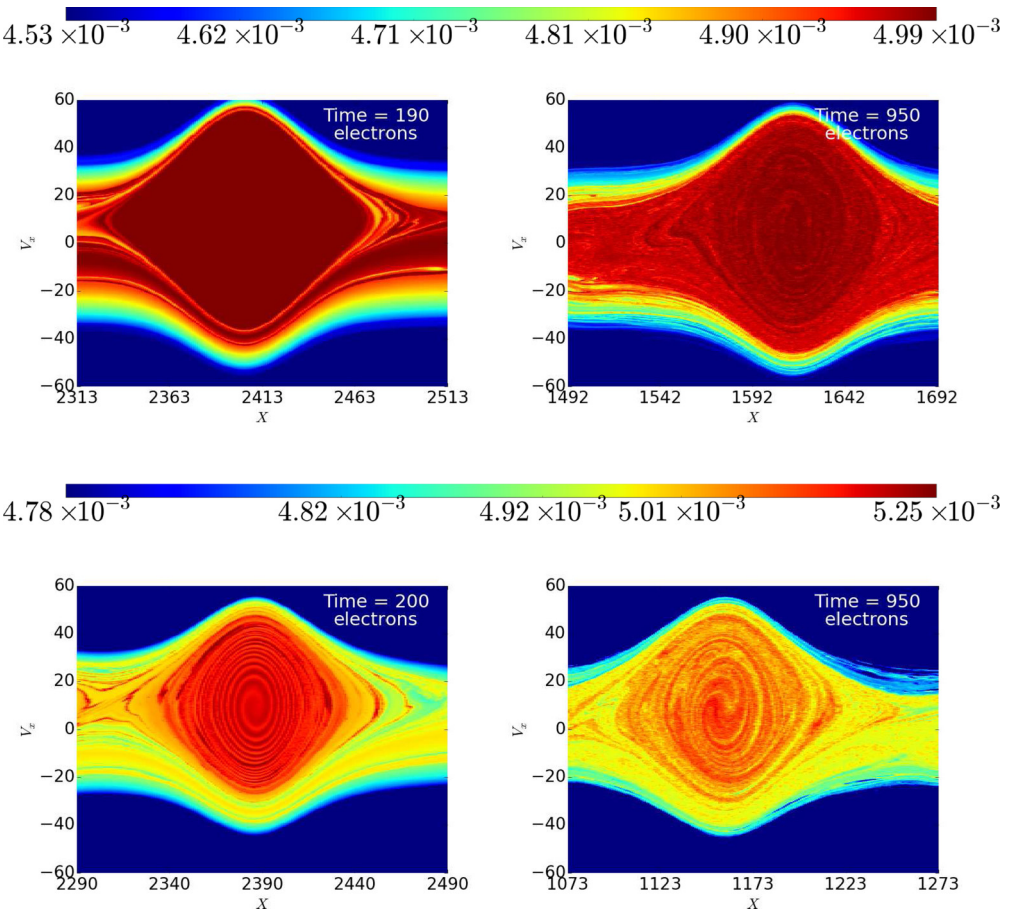

FIG. 8. For the case of large IDP, i.e., $\psi = 0.2$ and $\Delta = 500$, with $\beta = 0.0$ ($\beta = 0.2$), the electrons' distribution function are shown in the phase space in the two top (bottom) figures. These figures represent the trapping area associated with the right-propagating first and dominant IA soliton. The phase space structure of the plateau ($\beta = 0.0$) and the hump ($\beta = 0.2$) is presented before the first collision ($\tau = 190, 200$, respectively) and after the final collision ($\tau = 950$). Stability of IA solitons can be confirmed by comparing the size and shape of nonlinear structures. However, their symmetry is distorted due to the number of mutual collisions. Furthermore, plateau structure prove to be more robust than the other two shapes.

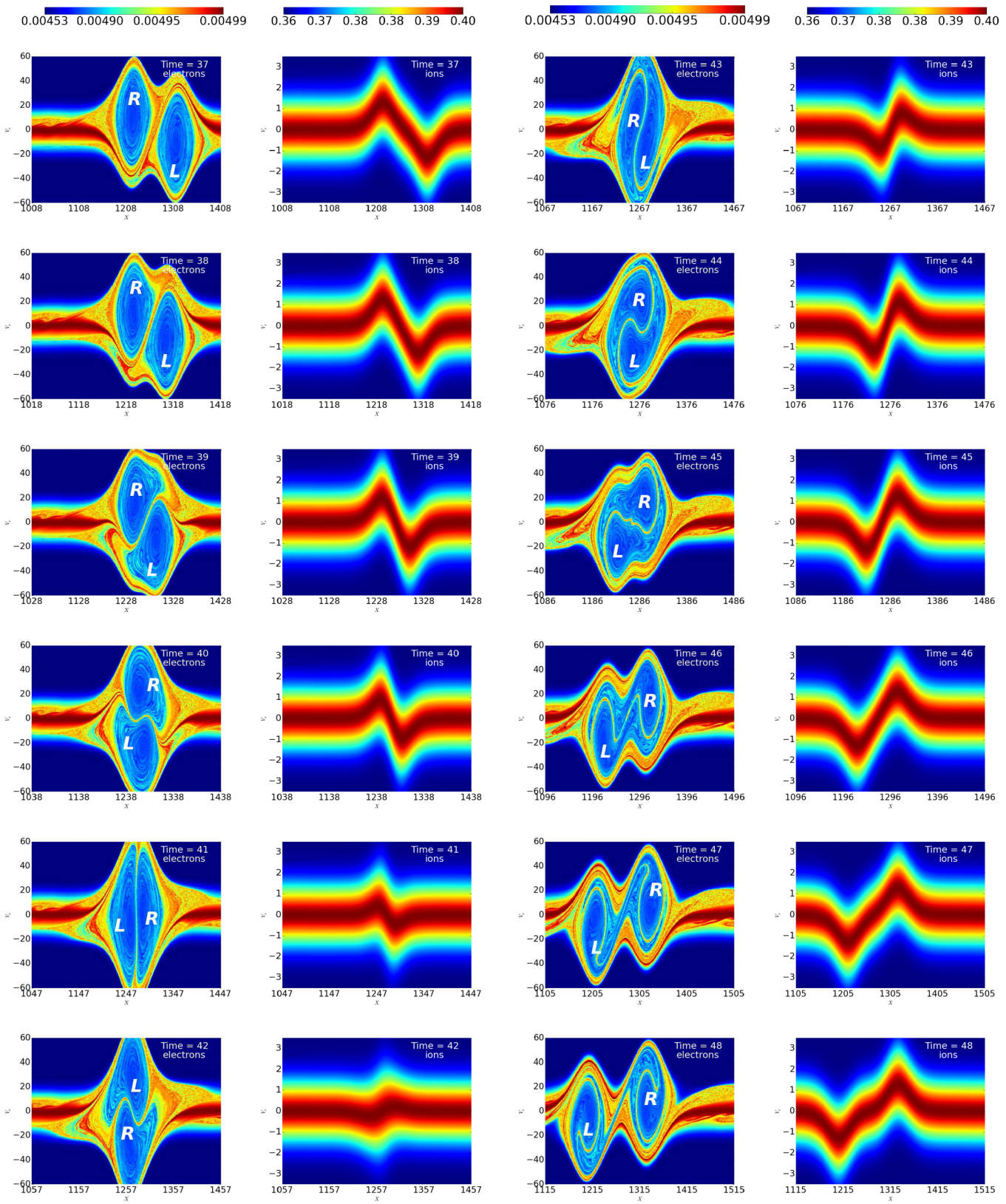

FIG. 9. Collision of hollows; for the case of $\beta = -0.1$, the distribution functions of electron and ions are presented during a collision between right (R) and left (L) propagating IA solitons. The frame is moving alongside the right-propagating IA soliton and shows the times from $\tau = 37$ up to $\tau = 48$ (arranged from top left corner). The collision for the electrons appears as a rotation of both phase-space hollows around their collective center of mass. Furthermore two solitons exchange a portion of their trapped population during collision. However, for the ions, the collision simply consists of two displacements moving through each other. See Supplemental Material [24] for complete successive steps of this collision, i.e., $0 < \tau < 130$.

For the kinetic level study, the temporal evolution of the distribution functions of plasma species are focused upon. Figure 7 displays the phase space structure of the electron distribution function at the same times as Fig. 6. The size and shape of the distribution function hollow accompanying the IA soliton remain intact, confirming the stability of velocity-direction features of IA solitons against mutual collisions. However, the symmetry of the distribution function inside the hollow is changing into a more and more chaotic form, as the IA soliton passes through more and more collisions.

Figure 8 provides the same results as Fig. 7 for two other cases, i.e., $\beta = 0.0$ and $\beta = 0.2$. The same tendency can be witnessed, the trapped population becomes more chaotic at the end of simulation compared to the initial step before the first collision. However, the internal structure of plateau structure ($\beta = 0$) displays less interruption compared to the two other forms, i.e., hollows and humps. Hence, we conclude that the plateau structure shows more resilience on the kinetic level during mutual collisions. This is due to the constant value of distribution function inside the plateau which can hide the spiral movement inside it. Moreover, the final snapshot of the hollow and humps at the end of simulations (after a few collisions) resemble the plateau distribution ($\beta = 0$) due to the increasing distortion in the trapped populations.

The same comparisons have been carried out for $-1 < \beta < 1$, specifically $\beta = -1.0, -0.5, 0.5$, and 1.0. This range of β covers all three regimes proposed by Schamel [8] as well as all three possible shapes of the trapped electrons distribution function. Hence, the stability of IA solitons, in the presence of trapped electrons, against successive mutual collisions is confirmed, which consequently proves Schamel's theory.

C. Collision process on kinetic level

In order to show the kinetic details of a collision between two solitons, we have carried out another set of simulations, in which the two oppositely propagating solitons are isolated from the chain formation simulation and are introduced into a new simulation box. Hence, the collision happens purely in pairs. This removes the effect of secondary phenomena coming from the chain formation process (such as wave packets, dribs, and other solitons) from the collisions. The time of extraction of the first soliton from the chain formation simulation is chosen $\tau < 200$, just before the first set of collisions.

Figure 9 presents the simulation results for the first collision between the two first/dominant IA solitons (marked as R and L) propagating oppositely for the case of $\beta = -0.1$, $\psi = 0.2$, and $\Delta = 500$. Due to the negative value of trapping parameter, IA solitons are accompanied by a *hollow* in electron distribution function. The right and left propagating IA solitons collide at time $37 < \tau < 42$. During this time they undergo one rotation around their collective center of mass. During collision, this rotation has been observed for all the other collisions of the first set of simulations (see Fig. 6) as well, e.g., $180 < \tau < 250$, $390 < \tau < 400$, $590 < \tau < 600$, and $790 < \tau < 800$. The rotation of the hollows in phase space around each other has been witnessed before in context of beam instability. Especially in the case of the two-beam instability, hollows in the phase space would attract each other, rotate and merge together two by two until they form one hollow [23]. Figure 9 also reports the phase space of ions and their behavior during collision, which is rather simple compared to electrons.

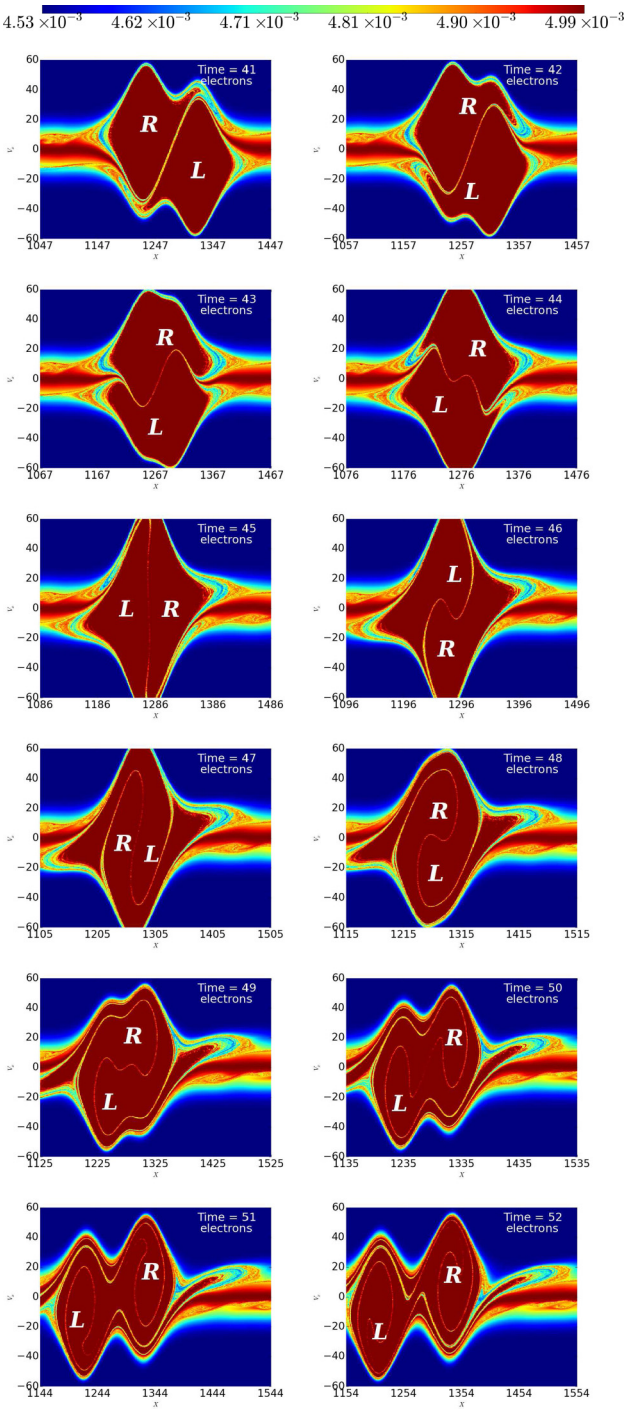

FIG. 10. Collision of plateaus; A collision between two IA solitons for the case of $\beta = 0.0$ is presented in the phase space of electrons from $\tau = 41$ up to $\tau = 52$ (starting from the top left corner). The collision takes place between right (R) and left (L) propagating solitons. The frame follows the right-propagating (R) soliton. The collision causes the two plateaus in the phase space to rotate once around their collective center and exchange some parts of their populations.

For a *plateau* accompanying the IA solitons, i.e., $\beta = 0$, the same pattern has been witnessed during their collisions as well (see Fig. 10).

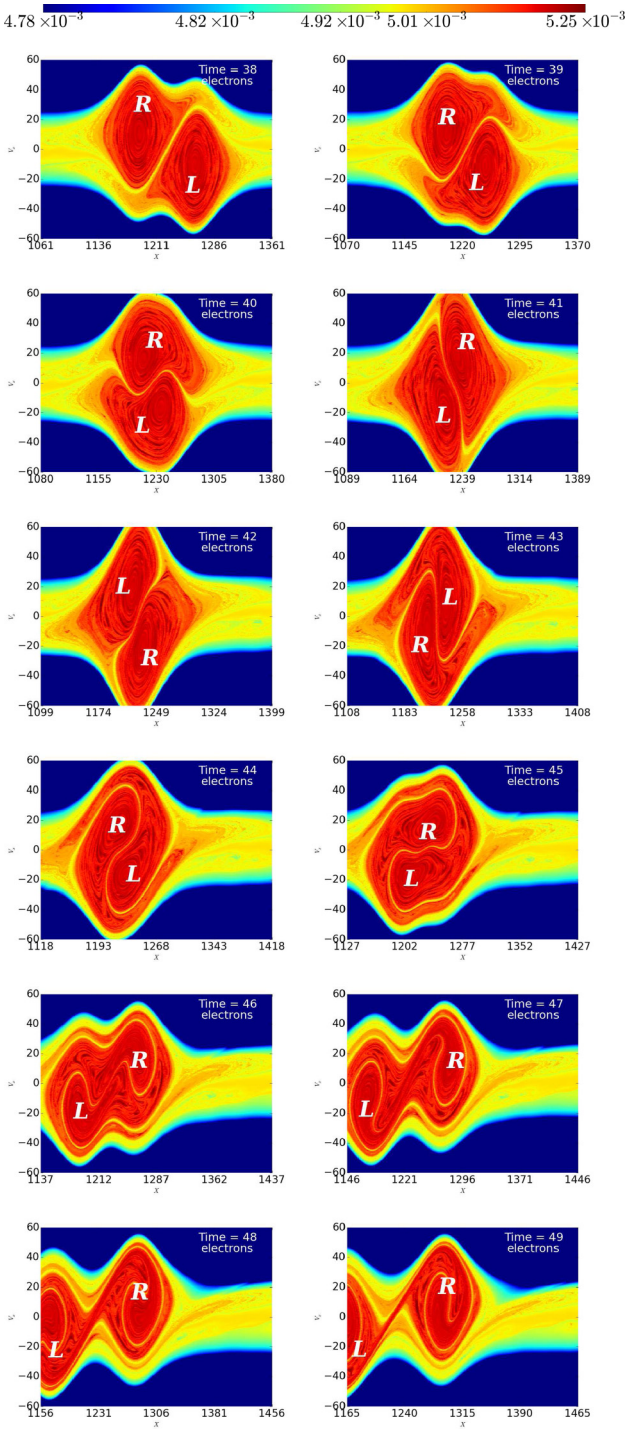

FIG. 11. Collision of humps; for the case of $\beta = 0.2$, a collision of two oppositely propagating IA solitons is shown in the phase space of electrons. The collision happens from $\tau = 40$ up to $\tau = 49$ (starting from the top left corner). The phase space structure accompanying the IA solitons are humps here, hence the red color. One rotation around the collective center and the exchange of trapped population takes place during collision between the two humps.

Figure 11 presents the results for the case of positive value of $\beta = 0.2$, when there is a hump in the electrons' distribution function following IA solitons. In cases of the other value of $-1 < \beta < 1$ (as far as considered here), the same pattern has been observed during the mutual collisions. We conclude that this rotational behavior of trapped populations stays independent from the value of trapping parameter (β).

Furthermore, in all the cases shown ($\beta = -0.1, 0, 0.2$) and studied ($-1.0 < \beta < 1.0$), during collision, the trapped populations of the two solitons are exchanged and shared during each collisions. This causes the internal structure of the accompanying nonlinear structures to change and reemerges more chaotic after each mutual collision (see Figs. 7 and 8). However, the smoothing (which is due to the discretization of the phase space on the both spatial and velocity direction) contributes to this phenomenon as well.

IV. CONCLUSIONS

A fully kinetic simulation approach is utilized to verify the Schamel's theoretical predictions concerning IA solitons in the presence of trapped electrons. This study confirms the stability of different features of these solitons against mutual collisions. Hence, this study concludes that kinetic effects such as electron trapping don't destroy IA solitons, at least in the range of β (trapping parameter) considered here. To the best of our knowledge, this study stands as the first attempt to address this issue purely based on kinetic theory.

The collisions (limited to the encounter of trapped electrons with the same trapping parameter) have been studied here on two levels, i.e., fluid and kinetic. On the fluid level, we have established that the IA solitons reemerge from the successive mutual collision intact. Four features of them, including hight, width, velocity, and shape, have been focused upon. The results of the analysis for $\beta = -0.1$ are reported here in which each soliton has experienced 12 mutual collisions. The constancy of these characteristics, under 10% fluctuation around the average values, implies the stability of IA solitons against mutual collisions.

On the kinetic level, it is presented that the overall shape and width of the trapped population accompanying the IA solitons does not change after a few mutual collisions. However, the internal structure of the trapped population changes after each collision without any traceable impact on the fluid-level characteristics. These changes push the phase space structures of the trapped populations to become more chaotic. We have noted that for $\beta \neq 0$, more prominent alteration has been witnessed.

Furthermore, the collision process itself, on the kinetic level, displays a more complicated behavior than what has been observed on the fluid level, i.e., two solitons simply passing through each other. Two main phenomena have been witnessed, i.e., rotation of the trapped populations around their collective center and the partial exchange of their trapped populations. These two procedures are shown to be independent from the value of trapping parameter (β). We have carried out simulations in which solitons are isolated from the chain formation process and have been introduced into a new simulation box in order to remove all secondary effects from collision process. The results confirm the same

pattern of behavior as the first set of simulations. The exchange of populations affects the internal arrangement of the trapped population and causes the alteration, which have been reported here. Nonetheless, the effect of smoothing contributes to the alteration.

Comparison of these results with the theoretical predictions for the collision of phase-space electron hollows should reveal the dynamical process behind the rotation during collisions. However, such a comparison and study stay beyond the scope of this paper. It is under consideration and will be communicated elsewhere. But this much can be mentioned here, that the results presented here are limited to moderate-size IA solitons and $-1.0 < \beta < 1.0$. In the case of high-amplitude IA solitons, the collision of IA soliton might be affected by the kinetic effects more strongly and the number of rotations (here equals one) might change.

ACKNOWLEDGMENTS

We are grateful to the anonymous referees for their helpful comments and constructive hints, which improved the paper extensively. This work is based upon research supported by the National Research Foundation and Department of Science and Technology. Any opinion, findings, and conclusions or recommendations expressed in this material are those of the authors, and therefore the NRF and DST do not accept any liability in regard thereto.

[1] H. Washimi and T. Taniuti, Phys. Rev. Lett. **17**, 996 (1966).
[2] H. Ikezi, R. Taylor, and D. Baker, Phys. Rev. Lett. **25**, 11 (1970).
[3] J. Pickett, J. Menietti, D. Gurnett, B. Tsurutani, P. Kintner, E. Klatt, and A. Balogh, Nonlinear Process. Geophys. **10**, 3 (2003).
[4] Y. Hobara, S. Walker, M. Balikhin, O. Pokhotelov, M. Gedalin, V. Krasnoselskikh, M. Hayakawa, M. André, M. Dunlop, H. Rème *et al.*, J. Geophys. Res.: Space Phys. **113**, A05211 (2008).
[5] J. Pickett, S. Kahler, L.-J. Chen, R. Huff, O. Santolik, Y. Khotyaintsev, P. Décréau, D. Winningham, R. Frahm, M. Goldstein *et al.*, Nonlin. Process. Geophys. **11**, 183 (2004).
[6] R. Hirota, Phys. Rev. Lett. **27**, 1192 (1971).
[7] R. Hirota, J. Phys. Soc. Jpn. **33**, 1456 (1972).
[8] H. Schamel, Plasma Phys. **14**, 905 (1972).
[9] H. Schamel, J. Plasma Phys. **9**, 377 (1973).
[10] H. Schamel, Phys. Scr. **20**, 306 (1979).
[11] A. Kakad, Y. Omura, and B. Kakad, Phys. Plasmas **20**, 062103 (2013).
[12] S. Sharma, S. Sengupta, and A. Sen, Phys. Plasmas **22**, 022115 (2015).
[13] X. Qi, Y.-X. Xu, X.-Y. Zhao, L.-Y. Zhang, W.-S. Duan, and L. Yang, IEEE Trans. Plasma Sci. **43**, 3815 (2015).
[14] B. Kakad, A. Kakad, and Y. Omura, J. Geophys. Res.: Space Phys. **119**, 5589 (2014).
[15] H. Schamel, Plasma Phys. **13**, 491 (1971).
[16] H. Schamel, J. Plasma Phys. **7**, 1 (1972).
[17] D. Nunn, J. Comput. Phys. **108**, 180 (1993).
[18] S. M. H. Jenab and I. Kourakis, Eur. Phys. J. D **68**, 1 (2014).
[19] S. H. Jenab and I. Kourakis, Phys. Plasmas **21**, 043701 (2014).
[20] H. Abbasi, M. H. Jenab, and H. H. Pajouh, Phys. Rev. E **84**, 036702 (2011).
[21] F. Kazeminezhad, S. Kuhn, and A. Tavakoli, Phys. Rev. E **67**, 026704 (2003).
[22] S. H. Jenab and F. Spanier, Phys. Plasmas **23**, 102306 (2016).
[23] V. Krasovsky, H. Matsumoto, and Y. Omura, Nonlin. Process. Geophys. **6**, 205 (1999).
[24] See Supplemental Material at http://link.aps.org/supplemental/10.1103/PhysRevE.95.053201 for the early stage development of the hollow and complete successive steps of a collision between two oppositely propagating hollows.